JOURNAL OF SPACECRAFT AND ROCKETS
Vol. 45, No. 2, March–April 2008

Improving Lunar Return Entry Range Capability Using Enhanced Skip Trajectory Guidance

Z. R. Putnam*
Georgia Institute of Technology, Atlanta, Georgia 30332
S. H. Bairstow†
Charles Stark Draper Laboratory, Inc., Cambridge, Massachusetts 02139
R. D. Braun‡
Georgia Institute of Technology, Atlanta, Georgia 30332
and
G. H. Barton§
Charles Stark Draper Laboratory, Inc., Cambridge, Massachusetts 02139

DOI: 10.2514/1.27616

The impending development of NASA's Orion crew exploration vehicle will require a new entry guidance algorithm that provides sufficient performance to meet all requirements. This study examined the effects on entry footprints of enhancing the skip trajectory entry guidance used in the Apollo program. The skip trajectory entry guidance was modified to include a numerical predictor–corrector phase during the atmospheric skip portion of the entry trajectory. A 4-degree-of-freedom simulation was used to determine the range capability of the entry vehicle for the baseline Apollo entry guidance and the predictor–corrector enhanced guidance with both high and low lofting at several lunar return entry conditions. The results show that the predictor–corrector guidance modification significantly improves the entry range capability of the crew exploration vehicle for the lunar return mission. The performance provided by the enhanced algorithm is likely to meet the entry range requirements for the crew exploration vehicle.

I. Introduction

IN 2004, the president of the United States fundamentally shifted the priorities of America's civil space program with the Vision for Space Exploration program, calling for long-term human exploration of the moon, Mars, and beyond [1]. This program focuses on returning astronauts to the moon by 2020 with the eventual establishment of a permanent manned station there. Experience gained from human exploration of the moon is then to be used to prepare for a human mission to Mars. To complete these tasks, a new human exploration vehicle, the Orion crew exploration vehicle (CEV), will be developed.

The NASA exploration systems architecture study (ESAS) selected a CEV similar to the Apollo program's command and service module, with a crewed command module and an uncrewed service module [2]. The CEV command module will be a scaled version of the Apollo command module (CM), maintaining the same outer moldline with a larger radius. In addition, the CEV will be required to return safely to land locations within the continental United States (CONUS) during normal operations, as opposed to the ocean landings performed in the Apollo program. Successful land recovery operations require an entry guidance algorithm capable of providing accurate landings over a large-area capability. Preliminary requirements indicate that the CEV entry vehicle must be capable of downranges of at least 10,000 km [3].

Long-range entries with downranges of 10,000 km can be easily achieved by moderate lift-to-drag ratio (L/D) blunt body entry vehicles, such as the CEV, by employing a skipping entry trajectory. When performing a skipping entry, the vehicle enters the atmosphere and begins to decelerate. The vehicle then uses aerodynamic forces to execute a pull-up maneuver, lofting the vehicle to higher altitudes, possibly exiting the atmosphere. However, enough energy is dissipated during the first atmospheric flight segment to ensure that the vehicle will enter the atmosphere a second time, at a point significantly farther downrange than the initial entry point. After the second entry, the vehicle proceeds to the surface. A longer-range trajectory is achieved in this manner, as shown in Fig. 1.

Skipping entries present a number of benefits and drawbacks. A skipping entry can provide an abort mode in the event of poor weather conditions at the primary landing site. The Apollo entry guidance included a skipping entry as a flight option for this reason. The long-range capability provided by a skipping entry may also simplify the entry phasing and targeting problem by allowing the vehicle to perform entry targeting within the atmosphere during entry, possibly saving propellant during in-space entry targeting. Most important, a skipping entry allows a moderate L/D vehicle, such as the CEV CM, to achieve anytime return from the moon when landing at a CONUS site. This ability significantly reduces the number of required landing sites for anytime return from the moon. Skipping entries also provide a number of technical challenges that must be addressed before a successful flight can occur. The long-range, long-duration nature of a skipping entry significantly increases the effects of navigation uncertainty at atmospheric interface, vehicle aerodynamic uncertainties, and atmospheric uncertainties. The entry vehicle's thermal protection system must also be able to withstand aerothermal load cycling and the higher integrated heat loads associated with a skipping entry. In addition to these challenges, skipping entry trajectories are inherently more complex and therefore typically have more complex abort modes, with few options for manual control in the event of a guidance failure.

Presented as Paper 7438 at the AIAA Space 2006 Conference, San Jose California, 19–21 September 2006; received 1 January 2007; revision received 11 June 2007; accepted for publication 12 June 2007.

*Graduate Research Assistant, School of Aerospace Engineering, 270 Ferst Drive. AIAA Student Member.
†Draper Fellow, Mission Design and Analysis, 555 Technology Square. AIAA Member.
‡Associate Professor, School of Aerospace Engineering, 270 Ferst Drive. AIAA Associate Fellow.
§Group Leader, Mission Design and Analysis, 555 Technology Square. AIAA Member.

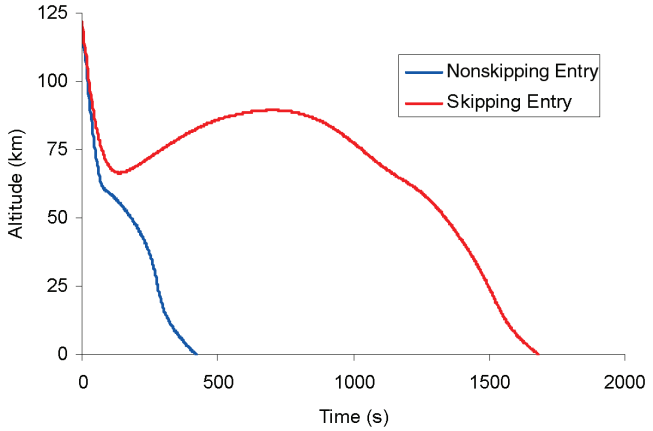

Fig. 1 Example of skipping and nonskipping lunar return entry trajectories.

The Apollo CM was capable of a maximum entry downrange without dispersions of 4630 km (2500 n mile) when employing the Kepler (ballistic) phase of its skip trajectory guidance [4]. However, this capability was never used. Studies for the first lunar outpost in the early 1990s used a 1.05-scale Apollo CM. These studies also employed the Apollo entry guidance algorithm and found a similar maximum downrange without dispersions of 4445 km (2400 n mile) [5]. However, in these studies, trajectories using the Kepler phase of the guidance were excluded from nominal trajectory design for the following reasons: desire to maintain aerodynamic control of the vehicle throughout entry, relative difficulty of accurate manual control to long-range targets in the event of a guidance failure, sensitivity to navigation and atmospheric uncertainties leading to inaccurate landings, and the absence of operational necessity for long-range entries [5]. Although these issues remain significant concerns for the design of the CEV entry system, preliminary requirements state that the CEV must be able to achieve a downrange of at least 10,000 km. Recent analyses indicate that the moldline of the CEV is fully capable of achieving downranges of this magnitude [6]. However, significant enhancements in the Apollo algorithm are required to maintain landed accuracy at these large nominal downranges.

II. Method

The range capability of the CEV entry vehicle was evaluated with a 4-degree-of-freedom simulation written in Matlab and Simulink. Entry trajectories were simulated over a range of flight-path angles, crossrange, and downrange commands using the baseline Apollo skip trajectory guidance and both high- and low-lofting predictor–corrector enhanced entry guidance algorithms. Uncertainty analysis was not included in this study, the objective of which is to demonstrate the feasibility of satisfying large nominal range targets for a moderate L/D CEV with an enhanced Apollo guidance algorithm.

A. Definitions

This study used the following definitions. Atmospheric interface, the altitude at which the entry vehicle enters the sensible atmosphere, was defined to be 122 km (400,000 ft) above the Earth's reference ellipsoid. Flight-path angle (FPA) refers to the entry vehicle's inertial flight-path angle at atmospheric interface. The inertial flight-path angle is the angle between the vehicle's velocity vector and the local horizontal, where negative values refer to angles below the horizon. Downrange is defined to be the in-plane distance traveled by the vehicle from atmospheric interface to landing. Crossrange is defined to be the out-of-plane distance traveled by the vehicle from atmospheric interface to landing. Miss distance is defined as the distance between the targeted landing site and the actual landing site. For the purposes of this study, an acceptable footprint was defined to be the region within which the CM achieved a miss distance of 3.5 km or less. This miss distance was chosen to allow for modest growth when navigation, aerodynamic, atmospheric, and vehicle uncertainties are included while still meeting program requirements.

B. Simulation

A computer simulation written in Matlab version 7.0.4 and Simulink version 6.2 was used to evaluate the skipping entry range performance of the CM. The equations of motion were integrated using Matlab's built-in Bogacki–Shampine ordinary differential equation integrator.

The Earth was modeled as a rotating oblate spheroid with a simple inverse-square gravity model. The Earth atmosphere was modeled with the standard U.S. atmosphere, 1962. This model was used to facilitate comparison with trajectory data from the Apollo program. Atmospheric wind was not modeled. The CM was assumed to be rotationally symmetric with a constant mass. The effects of reaction control system thrust (other than to rotate the vehicle), aerodynamic side force due to a nonzero sideslip angle, and shape change due to ablation were assumed to be negligible.

The simulation used 4 degrees of freedom, including all three spatial dimensions and the CM bank angle. The bank angle describes the orientation of the CM lift vector about the CM atmosphere-relative velocity vector. The CM is assumed to remain statically trimmed throughout entry based on a center-of-mass offset from the vehicle axis of symmetry.

The simulation was terminated when the CM either reached the ground (altitude equal to zero) or skipped out of the atmosphere (altitude above atmospheric interface of 122 km and velocity above circular orbital velocity of 7850 m/s).

A more complete description of the simulation can be found in [7].

C. Assumptions

Several assumptions were made for the analysis performed in this study. All entries were conservatively assumed to be posigrade equatorial. The entry state used is given in Table 1. The entry vehicle used was a scaled Apollo CM, as outlined in the ESAS [2], with a maximum diameter of 5.5 m. Apollo CM aerodynamics were used [8], and the vehicle was flown at trim angle of attack, generating an L/D of 0.4. Relevant entry vehicle properties are summarized in Table 2.

The vehicle was assumed to possess a thermal protection system capable of withstanding the extreme heating environment associated with high-velocity Earth entry. No explicit heating constraints were imposed on the trajectories in this study. However, the Apollo guidance algorithm effectively limits the maximum heat rate during entry to values that should be easily mitigated by ablative heat shield materials. The integrated heat load for a skipping trajectory is large due to the long time of flight. The effects of these large loads can be mitigated with proper insulation and other established techniques. Chapman's convective heating approximation [9] and the Tauber–Sutton approximation for radiative heating [10] were used to determine the laminar stagnation-point heat rate and heat load for all

Table 1 Vehicle entry state

Parameter	Value
Inertial velocity	11032 m/s
Altitude	122 km
Longitude	0 deg
Latitude	0 deg
Azimuth	90 deg

Table 2 Vehicle properties

Parameter	Value
Mass	8075 kg
Reference area	23.758 m^2
L/D	0.4

Table 3 Flight-path angle selections

FPA	Selection criteria
−5.635 deg	Center of aerodynamic corridor
−5.900 deg	Approximate shallow corridor boundary for EBE
−6.100 deg	Approximate steep corridor boundary for EBE

trajectories in this study. The maximum peak laminar stagnation-point heat rate and integrated heat load among all trajectories were approximately 260 W/cm^2 and 35 kJ/cm^2, respectively. In contrast, lunar Apollo missions had a maximum reference peak heat rate and integrated heat load of 392 W/cm^2 and 31.7 kJ/cm^2, respectively [11].

In addition, all entry trajectories complied with the deceleration requirements in NASA STD-3000 [12] and were assumed to provide acceptable deceleration environments.

D. Parameters Varied

Crossrange commands were varied between 0 km and 1000 km; downrange commands were varied between 1500 km and 13,000 km. This set of commands fully captured the range capability of the entry vehicle. Three flight-path angles were selected to examine vehicle capability over a set of atmospheric interface conditions, as shown in Table 3. Two of the FPAs were selected based on a CEV emergency ballistic entry (EBE) study conducted at the Charles Stark Draper Laboratory, Inc. in September 2005. Some failure modes for the CM may require ballistic entry. To ensure crew survival in such a failure mode, the CM skip entry corridor may be limited to a narrower ballistic entry corridor. This set of commands and FPAs was used with both the baseline Apollo entry guidance and the enhanced skip trajectory guidance.

A Monte Carlo analysis that incorporates navigation, aerodynamic, atmospheric, and vehicle uncertainties was not included in this study based on its objectives and for computational reasons. Over 900 entry trajectories required simulation to determine vehicle range capability at a sufficient resolution to locate infeasible regions at a single flight-path angle. Approximately 10–16 h of CPU time were required to run these 900 cases. A full Monte Carlo analysis would require 1000–3000 simulated entry trajectories per set of downrange and crossrange commands, significantly increasing the computational resources required to perform the analyses within a reasonable amount of time. These computational resources were not available for this study.

III. Results: Baseline Algorithm

A. Baseline Algorithm Description

The primary function of the entry guidance algorithm is to manage energy as the spacecraft descends to the parachute deploy interface. Energy management is accomplished through aerodynamic control of the vehicle. For a moderate L/D ratio capsule entry vehicle, aerodynamic control is achieved through lift modulation. Lift is modulated through bank angle control, for example, rotation about the vehicle velocity vector. Changing the vehicle bank angle changes the amount of lift in the vertical direction providing the means to manage vehicle energy. The baseline Apollo entry guidance algorithm uses bank angle control to modulate lift in decoupled longitudinal and lateral channels, with guidance cycles occurring at a frequency of 0.5 Hz.

Guidance's chief goal is to manage lift in the longitudinal channel so that the vehicle enters into the wind-corrected parachute deploy box at the appropriate downrange position. For a given FPA, full lift up provides maximum range, whereas full lift down provides the steepest descent. Lift down may be constrained by the maximum allowed g loads that can be experienced by the crew and vehicle. Any bank orientation other than full lift up or full lift down will result in a component of lift in the lateral channel. Crossrange position is controlled in the lateral channel by reversing the lift command into the mirror quadrant (e.g., +30 deg from vertical to −30 deg) once

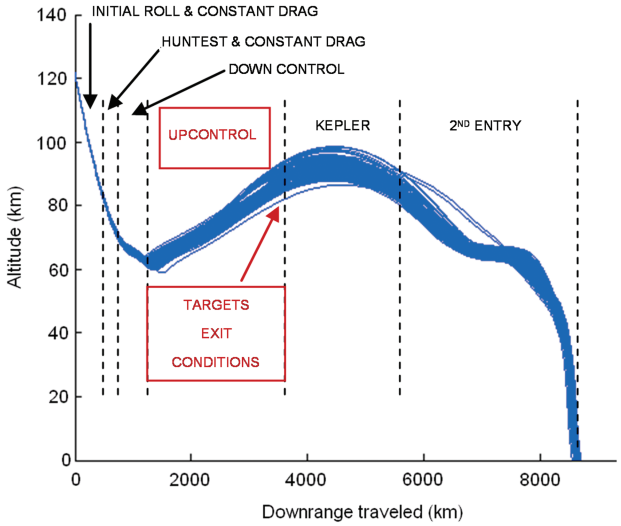

Fig. 2 Baseline algorithm entry guidance phases.

the lateral range errors to the target cross a threshold. The vehicle continues this bank command reversal strategy as it descends to the target. As the energy and velocity decrease, the lateral threshold is reduced so that the vehicle maintains control authority to minimize the lateral errors before chute deploy.

The baseline Apollo algorithm consists of seven phases designed to control the downrange position of the vehicle, as shown in Fig. 2.

1) Preentry attitude hold: maintains current attitude until a sensible atmosphere has been detected.

2) Initial roll: seeks to guide the vehicle toward the center of the entry corridor, nominally commanding the lift vector upward, otherwise commanding the lift vector downward to steepen a shallow entry.

3) Huntest and constant drag: begins once atmospheric capture is assured, triggered by an altitude rate threshold. This phase determines whether the vehicle will need to perform an upward "skip" to extend the vehicle's range, decides which of the possible phases to use, and calculates the conditions that will trigger those phases. The algorithm transitions to the downcontrol phase once a suitable skip trajectory is calculated; otherwise the algorithm transitions directly to the final (second entry) phase if no skip is needed.

4) Downcontrol: guides the vehicle to pullout using a constant drag policy.

5) Upcontrol: guides the vehicle along a reference trajectory, previously generated by the Huntest phase. This trajectory is not updated during the upcontrol phase. The algorithm transitions into the Kepler phase if the skip trajectory is large enough to exit the atmosphere; otherwise, the algorithm transitions directly into the final (second entry) phase.

6) Kepler (ballistic): maintains current attitude along the velocity vector from atmospheric exit to atmospheric second entry. Exit and second entry transitions are defined to occur at an aerodynamic acceleration of 0.2 g.

7) Final (second entry): guides the vehicle along a stored nominal reference trajectory, calculated preflight. Once the velocity drops below a threshold value, the algorithm stops updating bank commands and the guidance algorithm is disabled.

The Apollo guidance phases and phase-transition logic are discussed fully in [13].

B. Results Description

The results presented next are given in footprint plots. These plots show the miss distance associated with a particular downrange and crossrange command. Dark blue areas indicate accurate landings, whereas red areas indicate large miss distances. Light blue and dark blue areas provide acceptable accuracy, corresponding to miss distances of 3.5 km or less. Red areas denote miss distances of 10 km or greater, with some miss distances in excess of 1000 km.

C. Baseline Algorithm Results

The entry guidance algorithm used for the Apollo program was selected as the baseline algorithm for the CM entry guidance. Figures 3–5 show the landed accuracy over a range of downrange and crossrange commands for several FPAs (see Table 3). Figure 6 shows the footprint outlines at several FPAs.

Figure 3 shows the footprint for the baseline algorithm at an FPA of −5.635 deg. Maximum crossrange is approximately ±700 km.

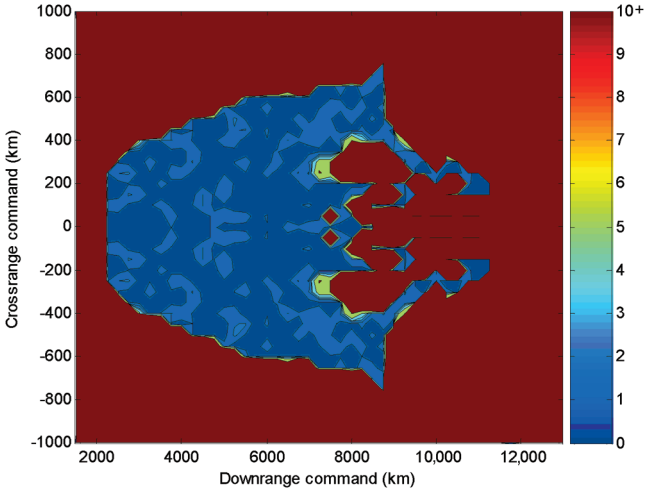

Fig. 3 Baseline miss distance (km) with FPA = −5.635 deg.

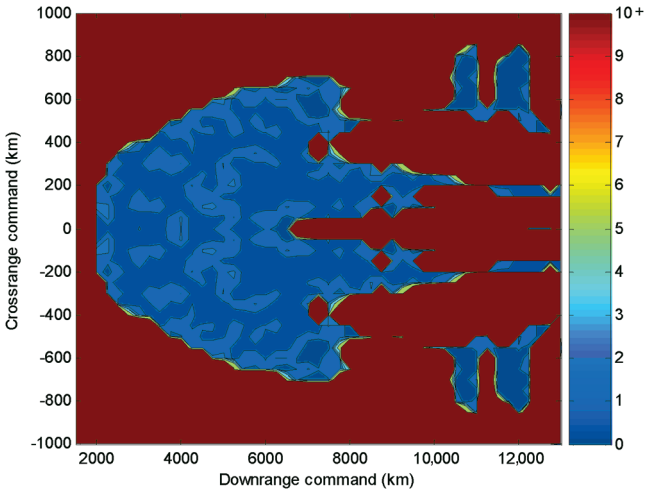

Fig. 4 Baseline miss distance (km) with FPA = −5.900 deg.

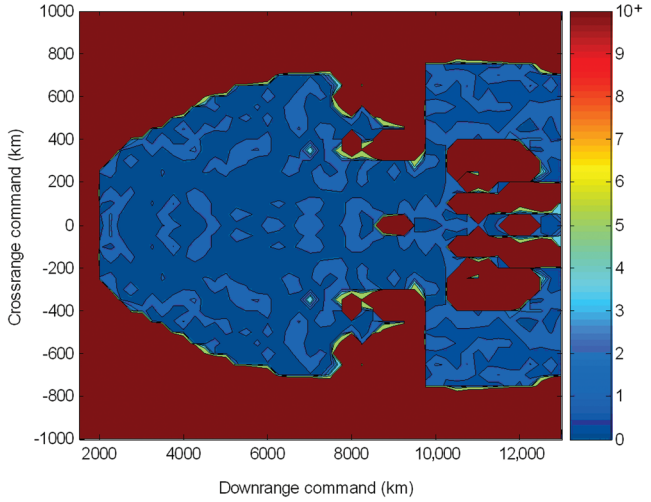

Fig. 5 Baseline miss distance (km) with FPA = −6.100 deg.

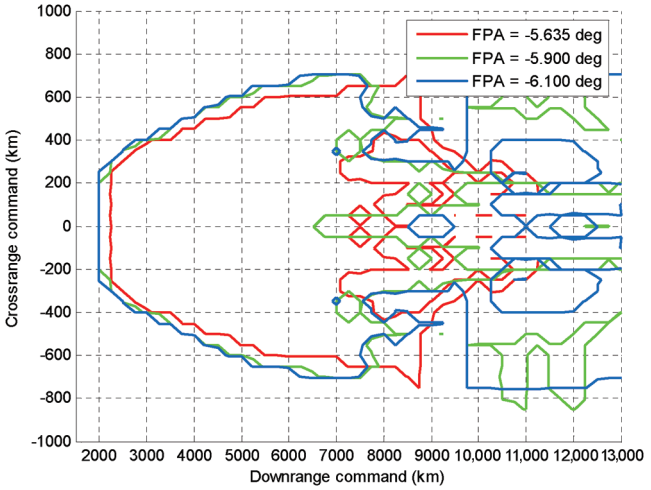

Fig. 6 Baseline range capability over several FPAs, miss distance <3.5 km.

Minimum downrange is 2250 km; maximum downrange is 7000 km. Within these ranges, the algorithm performs well. Figure 4 shows the footprint for the baseline algorithm at an FPA of −5.900 deg. Performance remains similar at this FPA. The minimum downrange decreases to 2000 km, whereas the maximum downrange remains 7000 km, with the exception of crossranges less than ±50 km. Some improvement is made in long-range performance, but accurate regions are patchy. Figure 5 shows the footprint for the baseline algorithm at an FPA of −6.100 deg. Significant performance improvements are visible at this FPA. Maximum downrange increases to 7500 km; minimum downrange is 2000 km. Maximum crossrange increases to ±750 km at large downranges. Long-range performance becomes accurate in two regions at crossranges greater than 400 km.

Overall, the baseline algorithm provides good performance over downrange commands between 2000 and 7000 km with crossranges up to 700 km, as shown in Fig. 6. However, improvement is required for long-range performance.

D. Rationale for Algorithm Improvement

Analysis of trajectories for long target ranges showed that the degradation of precision landing performance for the baseline Apollo algorithm occurred as the result of two issues. First, the upcontrol phase did not guide the vehicle to the desired exit conditions calculated by the Huntest phase. The control gains for the reference-following controller were likely designed with shorter target ranges in mind and did not achieve the intended results for the longest target ranges. Second, the exit conditions calculated by Huntest were inaccurate due to an outdated assumption. Because the baseline Apollo algorithm was designed for target ranges of less than 4600 km, the Kepler phase would always be short enough to ignore the effects of accumulated drag in the Kepler phase when calculating the exit conditions. For the much-longer target ranges intended for the CEV, this assumption is no longer valid. These two issues combined to cause severe undershoot in the longest target ranges.

IV. Results: Enhanced Guidance Algorithm

A. Enhanced Algorithm Description

The issues causing degradation in precision landing performance for long target ranges using the baseline Apollo algorithm were resolved by implementing three enhancements to the algorithm. First, the upcontrol and Kepler phases were replaced with a numeric predictor–corrector (NPC) algorithm, which targets the second entry conditions rather than the atmospheric exit conditions. This change in the guidance phase logic is reflected in Fig. 7. The NPC algorithm used for this purpose, PredGuid, is an aerocapture NPC guidance algorithm developed for the Aeroassist Flight Experiment. The PredGuid algorithm is described in [14]. An

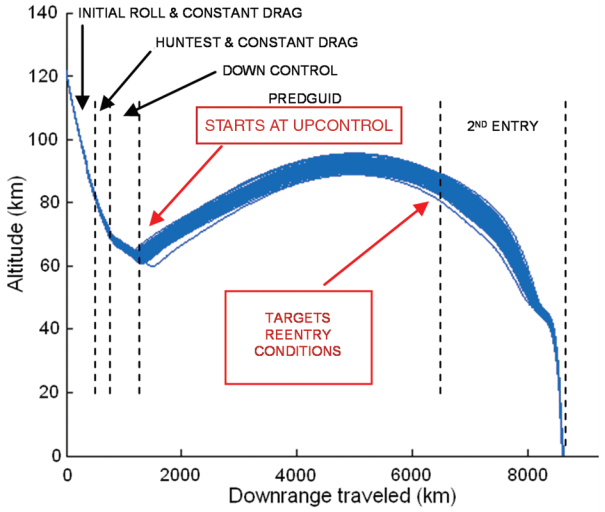

Fig. 7 Enhanced PredGuid entry guidance algorithm.

analytic predictor–corrector option was investigated but rejected due to the lack of a suitable closed-form expression to describe the entire skip trajectory.

Next, the final phase reference trajectory was redefined and extended to recenter it with respect to the CEV's range capability, because the CEV has different vehicle characteristics than the Apollo command module. Finally, the final phase range estimation method used by the Huntest and PredGuid phases was updated to enable the new final phase reference trajectory to support a wider spread of target ranges. More detail about the enhancements made to the algorithm is available in [7].

The effects of modulating the start time of the PredGuid phase was also investigated. A comparison was made between starting the PredGuid phase at the beginning of the upcontrol phase (as described) and starting the PredGuid phase at the beginning of the downcontrol phase. The difference in these two approaches resulted in different trajectory shaping, as shown in Fig. 8. Starting the PredGuid phase at the nominal time by replacing the upcontrol and Kepler phases resulted in a lower-altitude, shallower skipping trajectory, hereafter referred to as a low-loft trajectory. Starting the PredGuid phase earlier by also replacing the downcontrol phase resulted in a higher-altitude, steeper skipping trajectory, or high-loft trajectory.

B. Enhanced Algorithm Results

The results presented next detail the entry footprint of the CM using the enhanced numerical predictor–corrector guidance algorithm with both high and low lofting. Figures 9–14 show the landed accuracy, in terms of miss distance, of the CM at various downrange and crossrange commands for a given FPA. Figures 15 and 16 show the footprint outlines for high and low lofts for several FPAs.

Figure 9 shows the footprint for a low loft at an FPA of −5.635 deg. The CM achieves a maximum crossrange of approximately ±750 km. The minimum downrange is 2250 km,

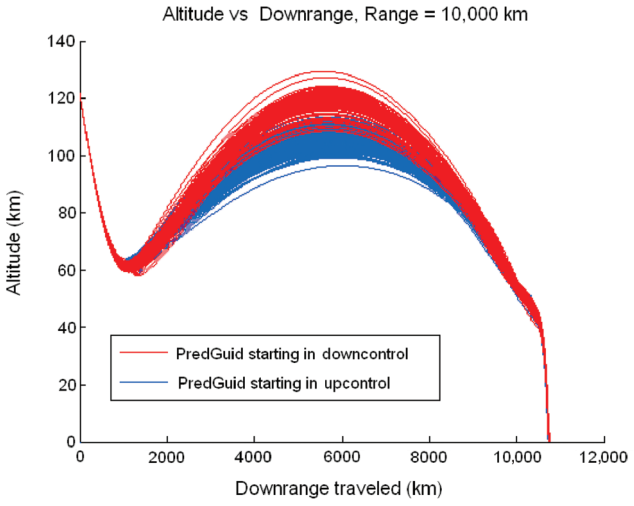

Fig. 8 PredGuid start in upcontrol and downcontrol produces low- and high-loft trajectories, respectively.

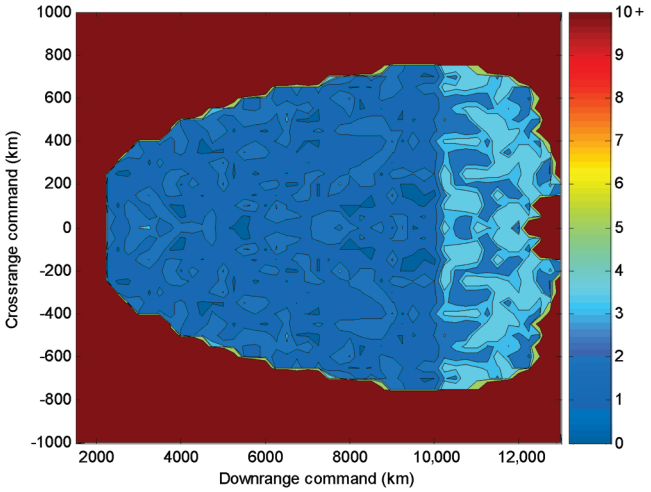

Fig. 9 Low-loft miss distance (km) with FPA = −5.635 deg.

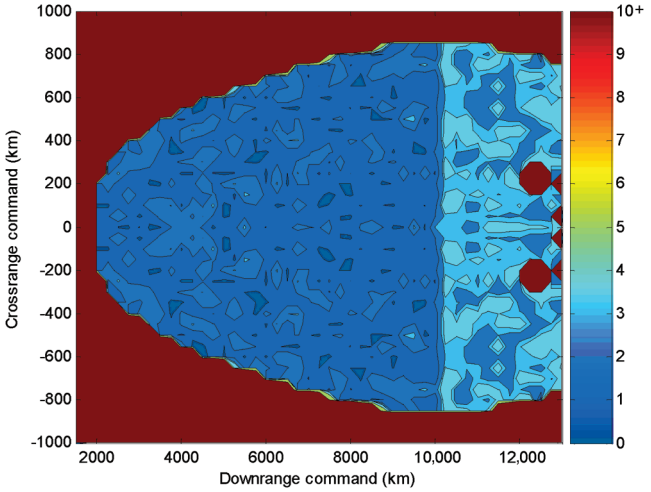

Fig. 10 Low-loft miss distance (km) with FPA = −5.900 deg.

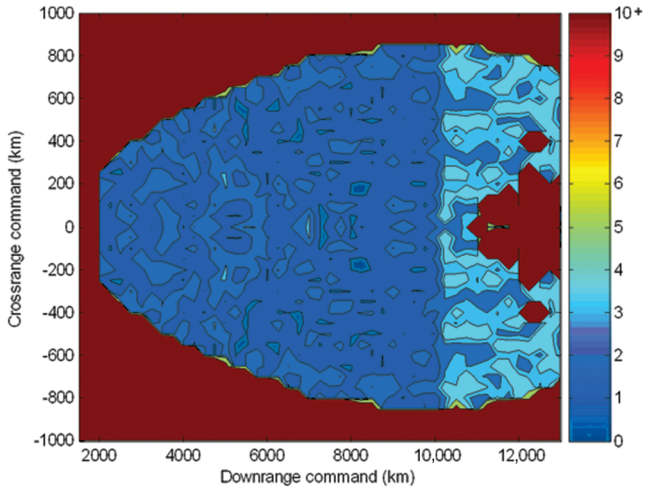

Fig. 11 Low-loft miss distance (km) with FPA = −6.100 deg.

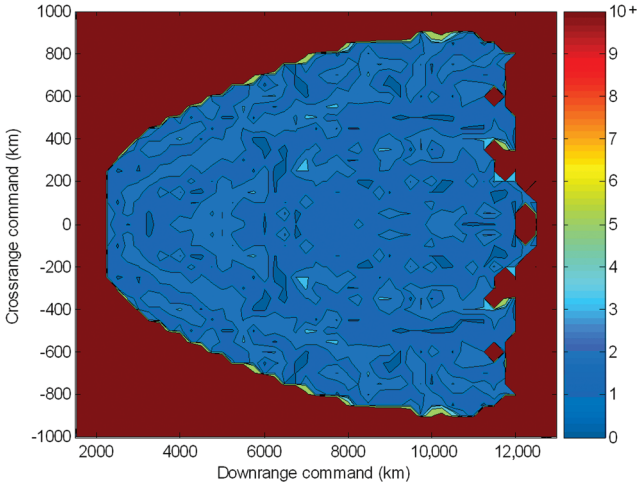

Fig. 12 High-loft miss distance (km) with FPA = −5.635 deg.

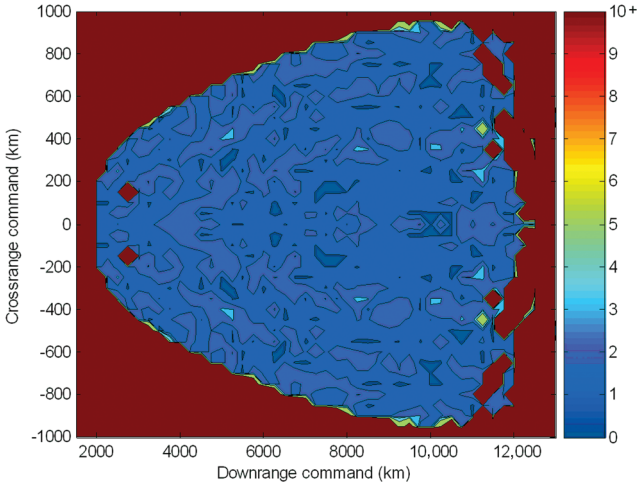

Fig. 13 High-loft miss distance (km) with FPA = −5.900 deg.

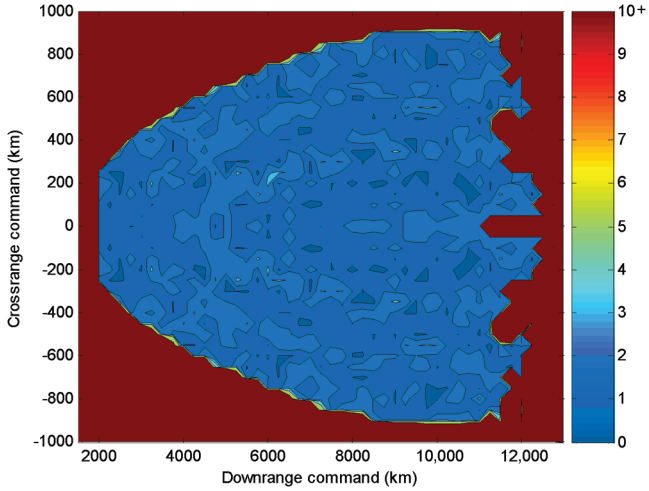

Fig. 14 High-loft miss distance (km) with FPA = −6.100 deg.

and significant accuracy is lost when downranges greater than 10,000 km are targeted. The footprint for a low loft at an FPA of −5.900 deg is shown in Fig. 10. The CM achieves a maximum crossrange of ±850 km, an increase of 100 km over the −5.635-deg case. The minimum downrange decreased to 2000 km from 2500 km in the −5.635-deg case. Significant accuracy is still lost when downranges greater than 10,000 km are targeted. The footprint for a

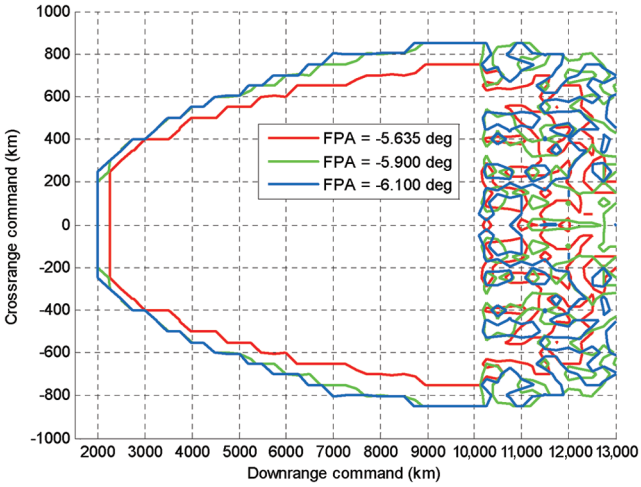

Fig. 15 Low-loft footprints for several FPAs, miss distance <3.5 km.

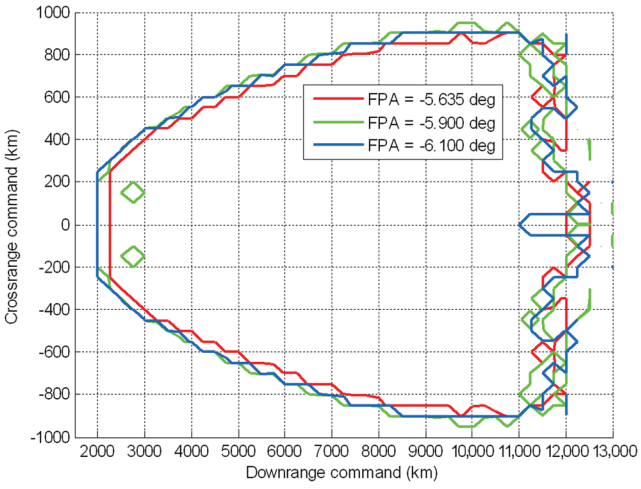

Fig. 16 High-loft footprints for several FPAs, miss distance <3.5 km.

low loft at an FPA of −6.100 deg is nearly identical to that of the −5.900-deg case (Fig. 11). Of note is the much larger red region starting at 11,000 km, indicating a deterioration of long-range performance with steepening FPA.

Figure 12 shows the footprint for a high loft at an FPA of −5.635 deg. The CM achieves a maximum crossrange of approximately ±900 km, a 150-km increase over the low-loft case. The minimum downrange is 2250 km and the maximum downrange is 11,250 km. No accuracy is lost between 10,000 and 11,250 km as in the low-loft case. The footprint for a high loft at an FPA of −5.900 deg is slightly better (Fig. 13). The CM achieves a maximum crossrange of ±950 km. The minimum downrange is 2000 km and the maximum downrange is 11,000 km, slightly less than the −5.635-deg case. Of particular note are two regions of inaccuracy near 3000 km downrange. Figure 14 shows the footprint for a high loft at an FPA of −6.100 deg. The CM achieves a maximum crossrange of ±900 km. Downrange performance is similar to the −5.900-deg case. The two inaccurate regions near 3000 km downrange have disappeared at this FPA.

Figures 15 and 16 show the footprints for low- and high-loft trajectories, respectively, at three FPAs. The footprint outlines correspond to miss distances of 3.5 km or less. As shown before, −5.900 and −6.100 deg provide similar performance, whereas −5.635 deg is slightly less capable. All trajectories begin to lose accuracy beyond 10,000 km. As in the low-loft cases, the performance of the high-loft −5.900- and −6.100-deg cases is similar, with the exception of the two inaccurate regions in the −5.900-deg case near 3000 km downrange. The −5.635-deg case is slightly less capable in minimum downrange and maximum

Table 4 Guided range performance summary

FPA	Minimum downrange	Maximum downrange	Maximum crossrange
		Baseline algorithm	
−5.635 deg	2250 km	7000 km	±700 km
−5.900 deg	2000 km	7000 km	±700 km
−6.100 deg	2000 km	7500 km	±750 km
		Low-loft enhanced algorithm	
−5.635 deg	2250 km	10,000 km	±750 km
−5.900 deg	2000 km	10,000 km	±850 km
−6.100 deg	2000 km	10,000 km	±850 km
		High-loft enhanced algorithm	
−5.635 deg	2250 km	11,000 km	±900 km
−5.900 deg	2000 km	11,000 km	±950 km
−6.100 deg	2000 km	11,000 km	±900 km

Table 5 Range capability improvement resulting from guidance algorithm enhancement over baseline Apollo algorithm

FPA	Maximum downrange improvement, %	Maximum crossrange improvement, %
	Low-loft enhanced algorithm	
−5.635 deg	42.9	7.1
−5.900 deg	42.9	21.4
−6.100 deg	33.3	13.3
	High-loft enhanced algorithm	
−5.635 deg	57.1	28.6
−5.900 deg	57.1	35.7
−6.100 deg	46.6	20.0

crossrange, but slightly more capable in maximum downrange, providing capability to 11,250 km.

These data show that, with the inclusion of the enhanced guidance algorithm, range performance is consistent over a large downrange and crossrange area. The shapes of the footprints are consistent with previous work performed with the Apollo CM. Over a range of FPAs, a crossrange of ±900 km is achievable with reasonable accuracy, whereas a downrange of 11000+ km is shown to be within the vehicle's capability. Table 4 provides a summary of the range performance data.

As shown in Table 4, there is no significant change in range capability within the set of FPAs examined. Miss distances of the CM remain within 3.5 km for low-loft trajectories with downranges less than 10,000 km. Miss distances of the CM remain within 3.5 km for high-loft trajectories with downranges less than 11,000 km, with the exception of two regions near 3000 km downrange at an FPA of −5.900 deg. These results represent a significant range capability extension over the baseline Apollo algorithm, as shown in Table 5.

At steeper FPAs with a low-loft trajectory, the maximum crossrange capability is increased slightly and the minimum downrange is decreased, both desirable effects. High-loft trajectories exhibit similar minimum downrange performance with increased maximum crossranges. Although the minimum downrange capability is better for steeper FPAs with high lofting, no clear advantage exists in crossrange performance for steep or shallow FPAs. A compromise between the high- and low-loft guidance algorithms could be implemented and may further decrease footprint dependence on FPAs.

V. Conclusions

The Orion CEV CM can achieve significant range capability improvements by replacing the Apollo upcontrol and Kepler phase guidance logic with a numeric predictor–corrector guidance algorithm. With this algorithm, the CM can robustly achieve a maximum crossrange of ±900 km, a maximum downrange of 10,000 km, and a minimum downrange of 2000 km while maintaining a landed accuracy within 3.5 km of the target. These ranges represent a 33–57% increase in maximum downrange and a 7–35% increase in maximum crossrange over the performance possible with the baseline Apollo guidance algorithm. Use of the enhanced guidance algorithm allows nominal landing sites to be located within most of the entry vehicle's considerable range capability. In addition, with the enhanced NPC algorithm, the Orion CEV CM range capability is largely independent of flight-path angle at atmospheric interface, providing mission design flexibility for human return from the moon.

Acknowledgments

This study was conducted with funding from the Charles Stark Draper Laboratory, Inc. The authors wish to acknowledge Steve Paschall (Charles Stark Draper Laboratory, Inc.) for his work in developing the simulation used in this study.

References

[1] Bush, G. W., "Remarks at the National Aeronautics and Space Administration," *Weekly Compilation of Presidential Documents*, Vol. 40, No. 3, 2004, pp. 66–68.

[2] Anon., "Exploration Systems Architecture Study Final Report," NASA TM-2005-214062, Nov. 2005.

[3] "NASA Solicitation: Conceptual Design of an Air Bag Landing Attenuation System for the Crew Exploration Vehicle," Langley Research Center Press Release, 14 Dec. 2005.

[4] Graves, C. A., and Harpold, J. C., "Reentry Targeting Philosophy and Flight Results from Apollo 10 and 11," Manned Spacecraft Center 70-FM-48, March 1970.

[5] Tigges, M., McCleary, B., Wood, R., Crull, T., Schmitt, L., Dawn, T., Langan, M., Wilson, S., Robertson, E., and Ondler, M., "Earth Land-Landing Analysis for the First Lunar Outpost Mission: Apollo Configuration," NASA JSC-25895, June 1992.

[6] Putnam, Z. R., Braun, R. D., Rohrschneider, R. R., and Dec, J. A., "Entry System Options for Human Return from the Moon and Mars," AIAA Paper 2005-5915, August 2005.

[7] Bairstow, S. H., "Reentry Guidance with Extended Range Capability for Low L/D Spacecraft," S.M. Thesis, Dept. of Aeronautics and Astronautics, Massachusetts Institute of Technology, Cambridge, MA, Feb. 2006.

[8] North American Aviation, Inc., "Apollo Technical Manual—Systems Dynamics Aerodynamic Data Manual," NASA CR-117277, Oct. 1964.

[9] Chapman, D. R., "An Approximate Analytical Method for Studying Entry into Planetary Atmospheres," NACA TN-4276, 1958.

[10] Tauber, M. E., and Sutton, K., "Stagnation-Point Radiative Heating Relations for Earth and Mars Entries," *Journal of Spacecraft and Rockets*, Vol. 28, No. 1, 1991, pp. 40–42.

[11] Pavlosky, J. E., and St. Leger, L. G., "Apollo Experience Report—Thermal Protection Subsystem," NASA TN D-7564, Jan. 1974.

[12] Anon., "Man-Systems Integration Standards," NASA STD-3000, Vol. 1, rev. B, July 1995.

[13] Morth, R., "Reentry Guidance for Apollo," Massachusetts Inst. of Technology Instrumentation Lab, Rept. R-532, Vol. 1, 1966.

[14] DiCarlo, J. L., "Aerocapture Guidance Methods for High Energy Trajectories," S.M. Thesis, Dept. of Aeronautics and Astronautics, Massachusetts Institute of Technology, Cambridge, MA, June 2003.

C. McLaughlin
Associate Editor